Pb-Pu Superlattices: An Example of Nanostructured Actinide Materials

Sven P. Rudin

Los Alamos National Laboratory, Los Alamos, New Mexico 87545, USA

(Received 12 December 2006; published 13 March 2007)

Density functional theory applied to Pb-Pu superlattices reveals two competing phases separated by a Mott transition between itinerant and localized $5f$ electrons. One phase, corresponding to Pu's bulk α phase, exhibits paired up Pu planes, thereby broadening the $5f$ bandwidth. Allowing spin polarization to emulate the energetics of electron correlation leads to another phase with larger volume, narrow $5f$ bandwidth, and more uniform local crystal structure, similar to bulk fcc Pu.

DOI: 10.1103/PhysRevLett.98.116401 PACS numbers: 71.27.+a, 61.46.−w, 68.65.Cd, 71.28.+d

The patterning of materials with nanometer-scale structures can strongly affect physical properties and in some systems even induce them (for example, Pd is paramagnetic in bulk but becomes magnetic in Pd-Ag quantum wells [1]). The effects change as the structural parameters vary, making it possible to fine-tune desired (or undesired) attributes. Such a fine-tuning could yield improved scientific understanding and greater technological control of actinide material characteristics. Aspects of particular interest among actinide solids include unique crystal structures [2], Mott transitions [3–6], strong anharmonicity [7–10], and strong electron-phonon coupling [11]. Many of these characteristics relate to the nature of the $5f$ electronic states as they vary from itinerant to localized. Designing nanostructures to tailor the $5f$ electron localization would allow fine-tuning of the associated properties.

In the light actinides the $5f$ electrons participate in bonding with a narrow bandwidth. Crystal-structure distortions broaden this bandwidth somewhat, pushing occupied energy levels down, which for the light actinides outweighs changes in the electrostatic energy and leads to crystal structures of low symmetry [12] and with itinerant $5f$ electrons. High-symmetry structures among the light actinides can be stabilized by going to high temperature. The most striking actinide, plutonium, exhibits six allotropes associated with temperature-dependent $5f$ localization. The crystal structures of Pu's low-temperature phases with itinerant $5f$ electrons, e.g., the monoclinic α phase, show significantly reduced symmetry compared to the cubic symmetry of the high-temperature phases. The technologically most important face-centered cubic (fcc) phase possesses mostly localized $5f$ electrons [13].

This work aims to assess the influence of nanoscale structures, specifically Pb-Pu superlattices, on the localization of plutonium's $5f$ electrons and associated properties. Both metals are highly toxic and have rarely been studied together [14], but of all elemental fcc metals Pb exhibits the closest lattice parameter to that of fcc Pu (6.5% mismatch). The fcc crystal structure provides the starting point for the nanostructures investigated here. The initial geometry places n_{ML} monolayers (ML) of fcc Pu next to the same number n_{ML} of fcc Pb ML. The layer stacking assumes the (001) direction; preliminary calculations indicate that stacking in the (011) direction leads to similar results. Periodic boundary conditions repeat this geometry in all dimensions. The simulation cells contain a single atom in each ML, which restricts the possible relaxations, though additional calculations with multiple atoms per ML indicate that lifting this restriction exhibits no advantage. Figure 1 shows the structures after relaxation using density functional theory (DFT) in the generalized gradient approximation (GGA).

DFT in the GGA accurately describes the complex crystal structure of Pu's low-temperature α phase but not the high-temperature fcc phase. The difference lies in the localization of $5f$ electron states: in the α phase all $5f$ electrons are itinerant; in the fcc phase some are itinerant and some are localized. The approximations in the exchange-correlation functionals of GGA and the local density approximation (LDA) cannot account for the strong correlations between electrons in a localized orbital. Successful approximate treatment of the variable $5f$ electronic state localization in Pu requires modifications to the GGA such as the introduction of magnetic moments [5,15–18] (i.e., going from a local density to a local spin density

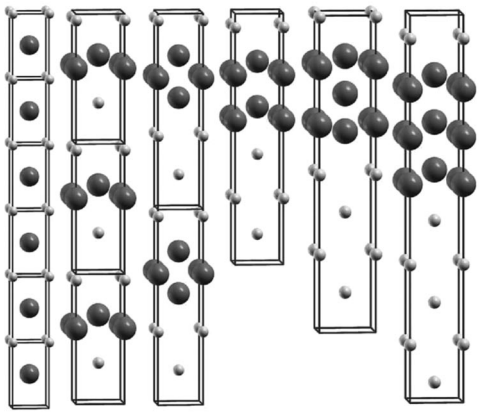

FIG. 1. Geometry of Pb-Pu superlattices for $n_{\mathrm{ML}} = 1, \ldots, 6$ after optimization without spin polarization. Small and large spheres represent Pb and Pu atoms, respectively; rods delineate the simulation cells.

approximation), an on-site Hubbard parameter in LDA + U [19–21] and dynamical mean field theory (DMFT) [22], or a split $5f$ manifold in the mixed level model [13].

Results presented here stem from DFT calculations in the GGA allowing magnetic moments, which emulates the correct treatment of electron-electron correlation in localized $5f$ electronic states. Allowing spin polarization in the GGA to DFT enables more electrons to occupy spatially different states, effectively keeping the electrons apart. One spin direction's electronic states shift relative to the other spin direction's, broadening the total electronic density of states (DOS), which can lower the total energy similar to crystal-structure distortions. This approach successfully describes the equilibrium volumes and bulk moduli of bulk Pu [18], which has sparked a debate as to whether high-temperature Pu phases are magnetic—to date, no magnetic moment has been experimentally observed [23]. The procedure cannot reproduce the large electronic specific-heat coefficient of fcc Pu, i.e., not all physical properties of Pu are adequately described. Nonetheless the approach also replicates the equilibrium structures and energetics of Pu compounds [24] and Pu alloys [25] and hence is appropriate to investigate the equilibrium structures and energetics of Pb-Pu superlattices. Refinements to this approximate treatment, orbital polarization and spin-orbit coupling, are not included here.

The projector-augmented wave (PAW) method [26] implemented in VASP [27,28] provides the DFT framework used here. The PAW method includes all electrons with the core electrons frozen in atomic states. Of the potentials supplied with VASP this work uses those that treat as valence electrons for Pb the $6s$ and $6p$ states and for Pu the $6s$ and $6p$ semicore and the $5f$, $6d$, $7s$, and $7p$ valence states. The Pu semicore states are included due to the short Pu-Pu bonds that appear between paired Pu planes (see below); bonds involving Pb atoms remain close to the Pb-Pb bond length of equilibrium bulk fcc Pb, so the Pb semicore $5d$ electrons are treated as core states (geometries and energy differences among small Pb-Pu superlattice systems change negligibly when the $5d$ electrons are treated as valence states). The PAW sphere radii are 1.69 Å and 1.57 Å for Pb and Pu, respectively, which leads to no overlap between spheres with the exception of a small overlap between Pu atoms for the shortest bonds. The PAW potentials use three and four nonlocal projectors for Pb and Pu, respectively; the plane wave energy cutoff is set to 320 eV. Exchange and correlation are treated in the GGA [29,30]. For each system the k-point mesh is refined until the total energy (calculated using the linear tetrahedron method with Blöchl corrections [31]) converges within 1 meV/atom.

The magnetic starting structures imposed on each system fall into one of three classes: nonmagnetic (NM), ferromagnetic (FM), or antiferromagnetic (AFM). The spins of all Pu atoms align in the FM case, while the AFM calculations are seeded with neighboring Pu planes having opposite spin directions. During optimization the FM/AFM spins remain unrestricted and retain their direction while adjusting their magnitude (final values fall in the range of 4.3–5.4μ_B/atom). The Pb spins are initiated similarly but consistently vanish. Imposing the AFM arrangement on pure bulk fcc Pu and using the DFT approach outlined above gives good agreement with the experimental volume; calculations of pure bulk fcc Pb without spin polarization reproduce the experimental lattice constant within a few percent. The results reported here include FM magnetic structures for completeness, but the discussion focuses on the NM and AFM cases which encompass the relevant physics as in bulk calculations.

In calculations that do not allow for energy lowering through spin polarization the superlattice lowers its energy by pairing Pu planes. This is analogous to calculations on bulk Pu without spin polarization where the low-symmetry α structure is favored over the highly symmetric fcc structure, though the two bulk structures cannot be related via a simple distortion. Figure 1 illustrates the Pu plane pairing juxtaposed with the Pb planes which remain very evenly spaced. The extent to which the Pu planes can pair up depends on n_{ML}: for even values of n_{ML} the monolayers close up in pairs much like atoms in the one-dimensional Peierls effect [32]. For odd n_{ML} not all monolayers can pair up, $n_{\mathrm{ML}} = 3$ in particular frustrates any pairing.

The distances between Pu atoms reveal another, remarkable likeness between the paired Pu planes and the bulk α-Pu phase. The α-Pu crystal structure's unit cell contains 16 atoms in eight unique environments; the low-symmetry monoclinic α structure appears completely unrelated to Pu's high-temperature fcc structure. The bonds between Pu atoms in the α phase split into two distinct length ranges: the short bonds, 2.42–2.53 Å, and the long bonds,

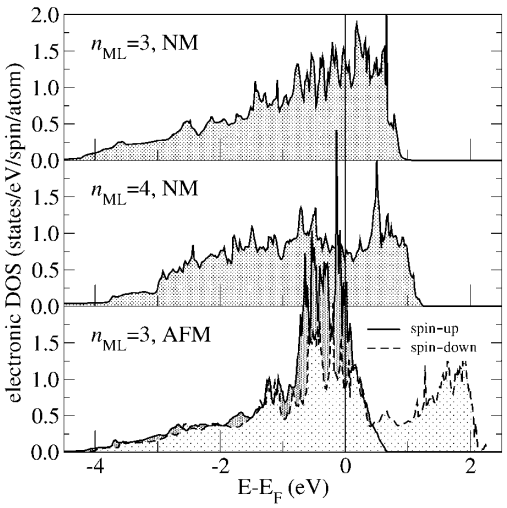

FIG. 2. Electronic DOS near the Fermi level for Pb-Pu superlattices. The top two panels show the DOS for two systems without spin polarization; the $n_{\mathrm{ML}} = 4$ system displays much larger crystal-structure distortions that drive states away from the Fermi energy. The lower panel shows the DOS for the $n_{\mathrm{ML}} = 3$ system with spin polarization.

3.21–3.56 Å (theoretical values). Surprisingly, in Pb-Pu superlattices similar ranges reappear between Pu atoms in paired planes, 2.48–2.56 Å, and between Pu atoms in unpaired planes, 3.08–3.31 Å. Such a similarity was not expected.

The pairing up of Pu planes affects the electronic DOS. Figure 2 contrasts the DOS of the frustrated $n_{\mathrm{ML}} = 3$ case with that of the successful $n_{\mathrm{ML}} = 4$ system. The pairing up of planes for $n_{\mathrm{ML}} = 4$ pushes states away from the Fermi E_F energy, thereby lowering the one-particle energy of occupied states near E_F. This energy lowering compensates for increases in the electrostatic energy much like crystal-structure distortions do in bulk light actinides.

Figure 2 also shows the DOS for $n_{\mathrm{ML}} = 3$ allowing spin polarization. Nearly all spin-up states in the valence band are occupied and form a narrow peak indicating they remain quite localized. Projecting out the f states shows that these in fact localize at the Pu sites and are of entirely one spin at a given site.

Calculations allowing spin polarization let the system lower its energy without the distortions present in the NM case, resulting in a much less dramatic dependence of the energy on n_{ML} as shown in Fig. 3. With the exception of $n_{\mathrm{ML}} = 1$, the energy of the AFM systems tends with n_{ML} towards the value obtained from averaging bulk fcc Pb and bulk fcc Pu (with AFM magnetic structure). Similarly the volume shows little dependence on n_{ML}.

The energies of the AFM and NM systems are quite close for even n_{ML}, i.e., when the NM system can lower its energy through plane pairing. The volumes, however, differ by 10%–20%. This ratio between two volumes of systems with similar energies is reminiscent of the two local minima in DMFT calculations of fcc Pu [22]. The DMFT volumes differ by 25%, as do the volumes of α and fcc Pu. Though the ratio of volumes in Pb-Pu superlattices is somewhat smaller than the DMFT and bulk ratios, the root cause appears to be the same Mott transition of the $5f$ electrons: either (i) plutonium sits in sites of low symmetry with the $5f$ electrons forming a somewhat broader band and participating strongly in bonding or (ii) Pu assumes highly symmetric sites with localized $5f$ electrons forming a narrow band.

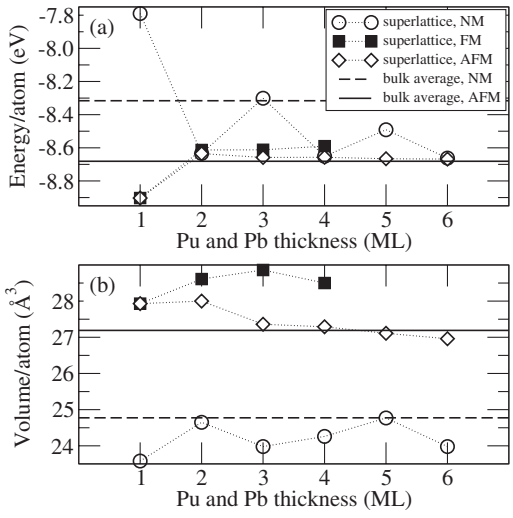

FIG. 3. (a) Energies and (b) volumes of Pb-Pu superlattices as a function of n_{ML} and imposed magnetic structure. The average energies and volumes stem from separate pure fcc Pu and pure fcc Pb calculations. Dotted lines are to guide the eye.

Creating Pb-Pu superlattices experimentally to observe the Mott transition of the $5f$ electrons may prove to be challenging. In addition to both metals being toxic and Pu being radioactive, atomically uniform layers with even n_{ML} do not appear unequivocally favorable. The $n_{\mathrm{ML}} = 1$ superlattice treated with spin polarization shows a significantly lower energy than the other superlattices. Similarly, for the $n_{\mathrm{ML}} = 2$ AFM superlattice the calculated energy drops by 0.13 eV/atom when rows of the two elements are interchanged at one Pb/Pu interface.

Figure 4 shows the spacing between planes for the Pb-Pu superlattices. The structures relaxed without spin polarization display the pairing up of Pu planes discussed above and also a hint of Pb planes pairing up. The $n_{\mathrm{ML}} = 3$ system again reveals frustrated behavior with the distance between Pu planes averaging the distances between paired and unpaired planes for $n_{\mathrm{ML}} = 4, 6$. Allowing spin polarization leads to much less dramatic geometries. As the layers gain in thickness the geometry in the center of the layers appears less influenced by interface effects and tends towards more bulklike regularity. The AFM Pu plane spacing tends towards just under 2 Å, corresponding to a lattice constant just under 4 Å, while the in-plane lattice constant remains near the calculated average of the elemental bulk

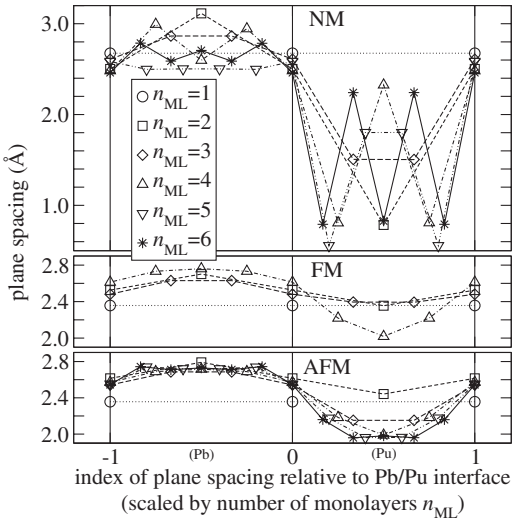

FIG. 4. Spacing between neighboring planes in Pb-Pu superlattices. Plane spacings are indexed starting from the Pb/Pu interface and scaled by n_{ML}. Pb/Pb plane spacings have scaled indices between -1 and 0; Pu/Pu plane spacings have scaled indices between 0 and $+1$. For comparison, the calculated plane spacing in bulk fcc Pb is 2.514 Å, while in bulk fcc Pu it is 2.072 Å (NM case) or 2.242 Å (AFM case). Lines connecting the symbols are to guide the eye.

TABLE I. In-plane lattice constant for Pb-Pu superlattices. The calculated pure bulk fcc lattice constants average to 3.39 Å.

	Magnetic structure		
n_{ML}	NM	FM	AFM
1	2.97 Å	3.44 Å	3.44 Å
2	3.33 Å	3.36 Å	3.27 Å
3	3.21 Å	3.40 Å	3.33 Å
4	3.34 Å	3.37 Å	3.31 Å
5	3.53 Å		3.34 Å
6	3.36 Å		3.34 Å

fcc values (see Table I). This makes the local environment for Pu atoms away from the interfaces that of a tetragonally distorted fcc crystal with a volume per atom very close to the bulk value. The layer thickness at which the tetragonal distortion becomes too costly in energy lies outside of what can be calculated with DFT.

In conclusion, DFT calculations on Pb-Pu superlattices indicate that these form nanostructures with two competing phases strongly related to the α and fcc phases of bulk plutonium. Unlike the bulk phases the superlattice phases transform into each other by an easily described distortion, the pairing of Pu planes. This pairing occurs with a volume collapse and a delocalization of the $5f$ electrons along the lines of the Mott transition associated with the bulk phases. Furthermore, the bond lengths between Pu atoms in paired and unpaired planes take on values very close to the short and long bonds of α-Pu. The two superlattice phases appear equally favorable in energy for even numbers of monolayers. Given that more accurate calculations of bulk Pu including orbital polarization for the correlation and spin-orbit coupling for relativistic effects lower the energy of fcc Pu, chances are that such a treatment of Pb-Pu superlattices would improve stability for the fcc-like phase. In essence, this would stabilize one of Pu's high-temperature allotropes at room temperature. Even with those additions the approach remains an approximate treatment; i.e., more accurate calculations and experimental verification are needed. While both elements' toxicity, Pu's radioactivity, and Pb's shielding properties make Pb-Pu superlattices unlikely candidates for technological applications, this system illustrates the rich potential in imparting actinide materials with nanostructures.

Many thanks go to Anders Niklasson, Eric Chisolm, and John Wills for helpful discussions. This research is supported by the Department of Energy under Contract No. W-7405-ENG-36.

[1] S. Mirbt, B. Johansson, and H. L. Skriver, Phys. Rev. B **53**, R13310 (1996).
[2] *The Chemistry of the Actinide Elements*, edited by L. R. Morss, N. M. Edelstein, and J. Fuger (Springer, New York, 2006).
[3] B. Johansson, Philos. Mag. **30**, 469 (1974).
[4] B. Johansson, Phys. Rev. B **11**, 2740 (1975).
[5] H. L. Skriver, O. K. Andersen, and B. Johansson, Phys. Rev. Lett. **41**, 42 (1978).
[6] S. Méot-Reymond and J. M. Fournier, J. Alloys Compd. **232**, 119 (1996).
[7] P. de V. du Plessis, G. H. Lander, A. M. Strydom, and B. Fåk, Physica (Amsterdam) **180–181B**, 321 (1992).
[8] J.-C. Marmeggi, G. H. Lander, R. Currat, and C. M. E. Zeyen, Physica (Amsterdam) **234–236B**, 129 (1997).
[9] M. E. Manley, B. Fultz, R. J. McQueeney, C. M. Brown, W. L. Hults, J. L. Smith, D. J. Thoma, R. Osborn, and J. L. Robertson, Phys. Rev. Lett. **86**, 3076 (2001).
[10] R. J. McQueeney, A. C. Lawson, A. Migliori, T. M. Kelley, B. Fultz, M. Ramos, B. Martinez, J. C. Lashley, and S. C. Vogel, Phys. Rev. Lett. **92**, 146401 (2004).
[11] M. J. Graf, T. Lookman, J. M. Wills, D. C. Wallace, and J. C. Lashley, Phys. Rev. B **72**, 045135 (2005).
[12] P. Soderlind, O. Eriksson, B. Johansson, J. M. Wills, and A. M. Boring, Nature (London) **374**, 524 (1995).
[13] O. Eriksson, J. D. Becker, A. V. Balatsky, and J. M. Wills, J. Alloys Compd. **287**, 1 (1999).
[14] D. H. Wood, E. M. Cramer, P. L. Wallace, and W. J. Ramsey, J. Nucl. Mater. **32**, 193 (1969).
[15] A. V. Postinov and V. P. Antropov, Comput. Mater. Sci. **17**, 438 (2000).
[16] Y. Wang and Y. Sun, J. Phys. Condens. Matter **12**, L311 (2000).
[17] A. M. N. Niklasson, J. M. Wills, M. I. Katsnelson, I. A. Abrikosov, O. Eriksson, and B. Johansson, Phys. Rev. B **67**, 235105 (2003).
[18] P. Soderlind and B. Sadigh, Phys. Rev. Lett. **92**, 185702 (2004).
[19] V. I. Anisimov, J. Zaanen, and O. K. Andersen, Phys. Rev. B **44**, 943 (1991).
[20] J. Bouchet, B. Siberchicot, F. Jollet, and A. Pasturel, J. Phys. Condens. Matter **12**, 1723 (2000).
[21] S. Y. Savrasov and G. Kotliar, Phys. Rev. Lett. **84**, 3670 (2000).
[22] S. Y. Savrasov, G. Kotliar, and E. Abrahams, Nature (London) **410**, 793 (2001).
[23] J. C. Lashley, A. Lawson, R. J. McQueeney, and G. H. Lander, Phys. Rev. B **72**, 054416 (2005).
[24] G. Robert, A. Pasturel, and B. Siberchicot, Phys. Rev. B **68**, 075109 (2003).
[25] B. Sadigh and W. G. Wolfer, Phys. Rev. B **72**, 205122 (2005).
[26] P. E. Blochl, Phys. Rev. B **50**, 17 953 (1994).
[27] G. Kresse and J. Furthmuller, Phys. Rev. B **54**, 11 169 (1996).
[28] G. Kresse and D. Joubert, Phys. Rev. B **59**, 1758 (1999).
[29] J. P. Perdew, J. A. Chevary, S. H. Vosko, K. A. Jackson, M. R. Pederson, D. J. Singh, and C. Fiolhais, Phys. Rev. B **46**, 6671 (1992).
[30] J. P. Perdew, J. A. Chevary, S. H. Vosko, K. A. Jackson, M. R. Pederson, D. J. Signh, and C. Fiolhais, Phys. Rev. B **48**, 4978 (1993).
[31] P. E. Blochl, O. Jepsen, and O. K. Andersen, Phys. Rev. B **49**, 16 223 (1994).
[32] R. E. Peierls, *Quantum Theory of Solids* (Clarendon, Oxford, 1955).